Journal of Power Sources 241 (2013) 112–120

Contents lists available at SciVerse ScienceDirect

Journal of Power Sources

journal homepage: www.elsevier.com/locate/jpowsour

Modeling and experimental validation of a Hybridized Energy Storage System for automotive applications

Simone Fiorenti [a,1], Jacopo Guanetti [a,1], Yann Guezennec [a,b], Simona Onori [a,*]

[a] Center for Automotive Research, The Ohio State University, Columbus, OH 43212, USA
[b] Mechanical and Aerospace Engineering Department, The Ohio State University, Columbus, OH 43212, USA

HIGHLIGHTS

- Experimental identification of equivalent electric circuit lead-acid battery model.
- Experimental identification of equivalent electric circuit supercapacitor model.
- Development of lead-acid battery + supercapacitor system for Start&Stop applications.
- Comparative analysis between battery vs. hybrid system for Start&Stop applications.

ARTICLE INFO

Article history:
Received 28 December 2012
Received in revised form
2 April 2013
Accepted 5 April 2013
Available online 22 April 2013

Keywords:
Circuit models
Dynamic models
Energy storage
Identification
Validation

ABSTRACT

This paper presents the development and experimental validation of a dynamic model of a Hybridized Energy Storage System (HESS) consisting of a parallel connection of a lead acid (PbA) battery and double layer capacitors (DLCs), for automotive applications. The dynamic modeling of both the PbA battery and the DLC has been tackled via the equivalent electric circuit based approach. Experimental tests are designed for identification purposes. Parameters of the PbA battery model are identified as a function of state of charge and current direction, whereas parameters of the DLC model are identified for different temperatures. A physical HESS has been assembled at the Center for Automotive Research The Ohio State University and used as a test-bench to validate the model against a typical current profile generated for Start&Stop applications. The HESS model is then integrated into a vehicle simulator to assess the effects of the battery hybridization on the vehicle fuel economy and mitigation of the battery stress.

1. Introduction

The trend in automotive market is nowadays toward the design of vehicles achieving better fuel economy and lower pollutant emissions. Several Hybrid and Plug-in Hybrid Electric Vehicles (HEVs and PHEVs) are now available on the market and are experiencing a fair commercial success, albeit they come with a significant increase in their powertrain complexity and cost, if compared to conventional vehicles [1]. On the other hand, Mild Hybrid Vehicles (MHVs) and the vehicles equipped with Start&Stop technology can still improve the fuel economy and reduce pollutant emissions, and are regarded as short and medium term solution.

In MHVs and Start&Stop applications PbA batteries play a dominant role for their lower cost and their simplicity of use. Nonetheless, more frequent engine starting and in some cases high charging currents due to regenerative braking can result in accelerated aging of the battery. Using a bigger battery or coupling the battery with another energy storage device could, in principle, mitigate those side effects. In this paper we look at the feasibility of a Hybridized Energy Storage System (HESS) involving PbA batteries and DLCs. Compared to PbA batteries, a typical DLC has higher power density but can store a lower amount of energy, as it is shown in Fig. 1. The underlying idea in the HESS is that the DLC delivers the high current peaks, while the battery processes only the average current.

In this paper, we propose a methodology for developing and experimentally identifying the models of the PbA battery and of the DLC. By connecting these two models in parallel, a model of the HESS is obtained, which is experimentally validated through tests designed with the purpose of reproducing the power requirements

* Corresponding author. Tel.: +1 614 247 1855; fax: +1 614 6884111.
E-mail addresses: simone.fiorenti@gmail.com (S. Fiorenti), jacopoguanetti@gmail.com (J. Guanetti), onori.1@osu.edu (S. Onori).
[1] These authors contributed equally to this work.

0378-7753/$ – see front matter © 2013 Elsevier B.V. All rights reserved.
http://dx.doi.org/10.1016/j.jpowsour.2013.04.017

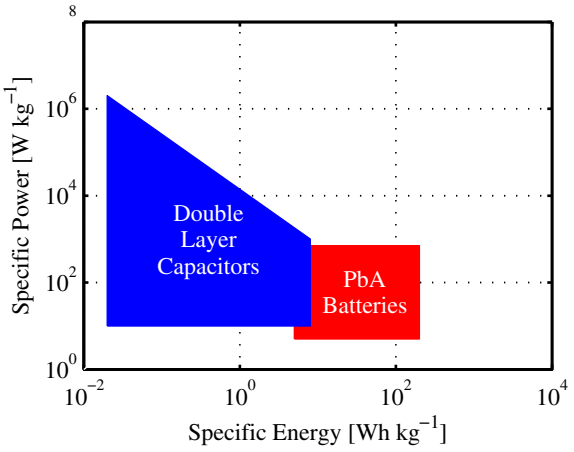

Fig. 1. Ragone plot for PbA batteries and DLCs [2].

of a vehicle equipped with the Start&Stop technology. The HESS model and the PbA battery model are integrated into a vehicle simulator; the operation of the vehicle is simulated both with the standalone PbA battery and with the HESS, and with and without the Start&Stop technology. The vehicle fuel economy and the battery stress are evaluated in these four different scenarios.

The paper is structured as follows: in Section 2 a brief introduction to the modeling problem of electrochemical devices such as batteries and DLCs is given; moreover, a review of some previous literature on HESSs consisting of PbA batteries and DLCs is discussed. Section 3 describes the experimental set-up used to test the PbA battery, the DLCs and the HESS. In Sections 4 and 5 the dynamic model of the PbA battery and the DLC are developed and experimentally identified. Section 6 describes the experimental validation of the HESS model. In Section 7 the model of the HESS is integrated in a vehicle simulator and the energetics of the energy storage systems are investigated through a simulation study. In Section 8 final remarks are discussed.

2. PbA battery, DLC and HESS modeling approaches

The PbA battery is the oldest type of rechargeable battery [3]. It is characterized by low energy density and relatively high power density. These features, the low cost and the simplicity of usage (no Battery Management System is needed) make PbA batteries well suited for automotive applications which do not involve a high degree of hybridization. Moreover, being the natural choice for conventional vehicles, in which the main requirement is to provide the cranking power to start the engine, PbA batteries are a good candidate for the lower levels of hybridization like Start&Stop and MHVs.

On the other hand, the DLC technology has come out over the last few decades. A DLC, also called supercapacitor or ultracapacitor, is an electrochemical device with extremely higher energy density compared to a conventional capacitor [4]. Its power density, although generally lower than the conventional one, is still significantly higher compared to batteries, as shown in Fig. 1. This feature makes it well suited for all those applications which require high levels of power without demanding a high level of energy and it can conveniently be used together with other devices, such as batteries, to increase their power capability.

Modeling PbA batteries [5–7] and DLCs [8–14] has been the subject of extensive research over the past decades.

Approaches to both PbA batteries and DLC modeling can be divided in three groups: electro-chemical models, data-driven models and equivalent circuit based models.

Manufacturers may use sophisticated, high order electrochemical models in order to improve the design of new devices [15,16]; although the device's behavior is well represented over a wide operating range, the complexity of the model itself makes this type of modeling approach unsuitable for the purpose of the present work.

Data driven models have been proposed (for instance, [14]) that do not have an *a priori* model structure or a direct physical meaning. The structure and the values of the parameters are tuned in order to get the best fitting of the experimental data. The data-driven approach generally leads to high order models and requires a large amount of data and computational resources.

Finally, the modeling approach which best meets the needs of this work is the one based on equivalent electric circuit representation of the devices. The order of the model is usually selected so as to have a good trade-off between accuracy and complexity [17–22].

The main objective of this work is the modeling of an HESS intended for Start&Stop applications, capable on one side to capture the most significant electrical dynamics of the systems and be reasonably accurate over the operating range of relevance, and on the other side to be simple enough to keep the parameter identification effort low.

In this work the choice is to use a 1st order equivalent circuit model for the battery (discussed in Section 4) and a 2nd order model for the DLC (discussed in Section 5) thus turns out to be a good compromise between complexity (from both the identification and the simulation standpoint) and accuracy over a reasonable time scale.

HESSs for automotive applications have been fairly studied in the last decade. They may be categorized into passive HESSs and actively controlled HESSs; the former are simply the parallel connection of a battery module and a DLC module, whereas the latter also involve a power electronic interface which actively controls the power flow between battery, DLC and load.

Passive HESSs consisting of a PbA battery and a DLC are investigated in Refs. [23,24], where simple models are used to size the components and analyze the interactions between battery and DLCs.

Actively controlled HESSs have been studied in more detail in the literature. HESSs consisting in PbA batteries and DLCs are investigated in Refs. [19,25–28]. In these works, the applications range from simple on-vehicle energy storage to solutions for battery life extension.

Not only PbA batteries, but also Li-ion batteries have been proposed for the usage in HESSs. In Refs. [29–32] an actively controlled Li-ion battery – DLC hybrid system for portable applications was investigated. Ref. [33] investigates the energy-power performance of an active HESS involving Li-ion batteries, intended for pulsed applications. On the other hand, [11] presents an identification method for both the Li-ion battery and the DLC, based on Electrochemical Impedance Spectroscopy.

Although a fair amount of work has been done on HESSs, with particular regard to actively controlled HESSs, a straightforward methodology for the modeling and experimental validation of a passive PbA battery-DLC HESS is still lacking.

3. Experimental set-up

The experimental set-up used to test a PbA battery, a DLC and a HESS is shown in Fig. 2. It consists of a programmable power supply, an electronic load, an environmental chamber, a data acquisition board, a computer and current, voltage, temperature sensors. The power supply and the electronic load are connected in parallel and remotely controlled through a PC; the current profile is submitted to the equipment through a LabView interface and actuated by either the supply or the load, depending on the current charge/discharge event.

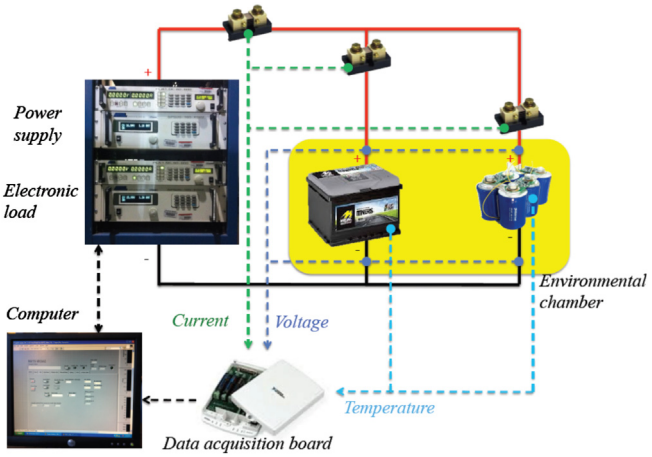

Fig. 2. Experimental set-up.

Available measurements are battery current (i_{batt}), DLC current (i_{dlc}) and the overall HESS current (i), the battery voltage (v_{batt}), and the 6 DLC cells voltages (v_{dlc}), the surface temperatures of the battery (T_{batt}) and DLCs (T_{dlc}). All of the sensed signals are acquired through an acquisition board[2] which sends the digitalized measurements to the PC, where they are displayed and stored.

The battery model identification and validation are conducted for the 12 V PbA sealed battery MIDAC Itineris 3 shown in Fig. 3, whose specifications are shown in Table 1.

The Maxwell BCAP1500 DLC, shown in Fig. 4, was selected for this work, whose electrical and thermal features are summarized in Table 2.

4. PbA battery

An identification test is specially designed for the identification of the battery model parameters. The identification test, named Pulse test, implemented in this work comprises of current pulses superimposed to the constant discharge/charge profile to excite the battery dynamics at different SoC. In addition to the pulse test, a capacity test followed and proceeded by a full charge is also concluded to assess the actual battery capacity. All tests, both the Pulse and Capacity test and the Charging protocol are performed in an environmental chamber at 25 °C.

4.1. Capacity test and charging protocol

The purpose of the capacity test is to evaluate the actual capacity of the battery. The test is performed in an environmental chamber at 25 °C and at least 12 h after a full charge. The battery is discharged at a constant C/20 C-rate (3.6 A). The discharge is interrupted as soon as the voltage drops below 10.5 V.

The charging protocol is as follows: the battery is charged for 23 h with a Constant Current/Constant Voltage strategy, with 25 A maximum current and 16 V maximum voltage. The charge continues for 1 h at 7.2 A constant current.

4.2. Pulse test

The purpose of the pulse test is to get significant data for the identification of the battery model. The test is performed in an environmental chamber at least 12 h after a full recharge. The battery operates at overall 35% depth of discharge (DoD). It is first discharged from 100% to 65% SoC and then recharged from 65% to 100% SoC. The discharge/charge phases are at constant C/20 C-rate (3.6 A). During both the discharge and charge phases, a 1C pulse event is superimposed at given SoC, namely, 95%, 85%, 75%, 65% in discharge and 75%, 85%, 95% in charge, as shown in Fig. 5. Fig. 6 shows the pulse event at 65% SoC; every pulse event has the same current profile, which consists of:

- 60 s of relaxation (0 A);
- 20 s of discharge at 1 C (72 A);
- 60 s of relaxation (0 A);
- 20 s of charge at 1 C (72 A);
- 60 s of relaxation (0 A).

[2] The SCC Modules are in SCC-68 Carrier, connected to PCI-6221 32-bit DAQ card in a Windows PC.

Fig. 3. MIDAC Itineris LN3.

Table 1
MIDAC Itineris LN3 data-sheet[34].

MIDAC Itineris 3	
Capacity [Ah]	72
Nominal voltage [V]	12
Cold cranking current [A]	640
Starting power (10 s at −18 °C) [kW]	5
Energy content (20 h at 25 °C) [Wh]	870

Fig. 4. Maxwell BCAP1500.

Table 2
Maxwell BCAP1500 data-sheet [35].

Maxwell BCAP1500	
Capacitance (2.7 V, 25 °C) [F]	1500
Rated voltage [V]	2.7
Equivalent series resistance [mΩ]	0.47
Operating temperature [°C]	−40 to 65
Cyclability	10^6
Energy density [Wh kg^{-1}]	5.4
Power density [W kg^{-1}]	6600
Thermal resistance (R_{th}) [°CW^{-1}]	4.5
Thermal capacitance (C_{th}) [J °C^{-1}]	320

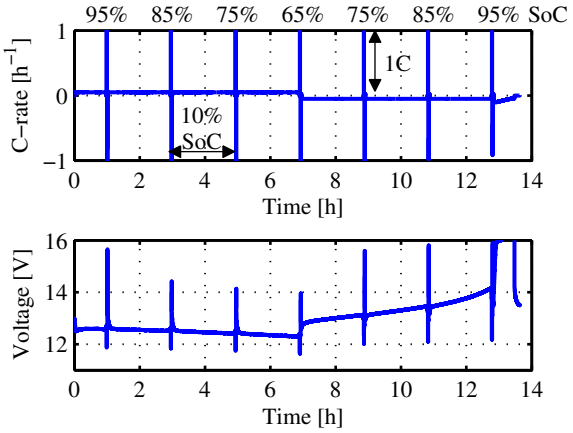

Fig. 5. Battery pulse test current and voltage profiles.

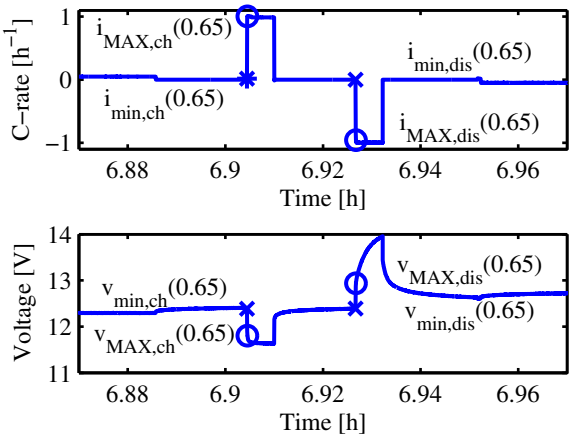

Fig. 6. Current and voltage profile during the pulse event at 65% SoC, with the variables used in R_0 calculation in Equation (3).

4.3. PbA battery parameter identification

The PbA battery is modeled with a 1st order Randles model with hysteresis depicted in Fig. 7. The battery SoC dynamics are given by:

$$\mathrm{SoC}(t) = -\frac{i_{\mathrm{batt}}(t)}{3600 Q_{\mathrm{batt}}} \tag{1}$$

where i_{batt} is the current flowing in the battery, assumed positive when discharging the battery and negative when charging, and Q_{batt} [3] is the nominal battery capacity.

Applying Kirchhoff Voltage Law to the circuit in Fig. 7, the voltage at the battery terminals is:

$$v_{\mathrm{batt}}(t) = v_{\mathrm{oc}}(\mathrm{SoC}) + h(t) - R_0(\mathrm{SoC}) i_{\mathrm{batt}} - v_1(t) \tag{2}$$

In Equation (2), v_{oc}(SoC), $h(t)$, R_0(SoC) are model parameters to be identified together with the parameters R_1 and C_1 of Fig. 7.

4.3.1. R_0 identification

The R_0 resistor models high frequency voltage variations. At each current pulse of the pulse test an estimation of R_0 is obtained as:

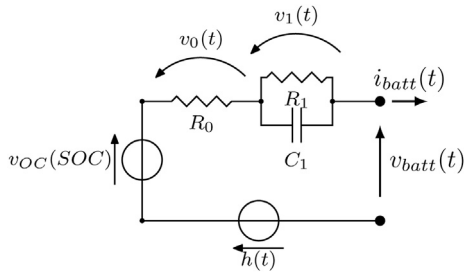

Fig. 7. 1st order Randles battery model with hysteresis.

$$R_{0,q}(\mathrm{SoC}) = \frac{v_{\mathrm{MAX},q}(\mathrm{SoC}) - v_{\mathrm{min},q}(\mathrm{SoC})}{i_{\mathrm{MAX},q}(\mathrm{SoC}) - i_{\mathrm{min},q}(\mathrm{SoC})} \tag{3}$$

where the meaning of v_{MAx}, v_{min}, i_{MAx}, i_{min} is explained in Fig. 6 and the subscript q is q = [ch,dis]. The estimates of R_0(SoC) in charge and in discharge are plotted in Fig. 8

4.3.2. v_{oc} identification

v_{oc}(SoC) is the open circuit voltage, also called *relaxation curve*; it is the voltage reached by the battery after a *full rest* and is a monotonically increasing function of SoC. The v_{oc} can be either experimentally evaluated[4] or identified.

For this work we obtain the v_{oc} via model identification from the C/20 constant current tests. Fig. 9 shows the v_{oc}(SoC) curves obtained. The value of v_{oc} used in the model is selected to be either the charge or the discharge v_{oc}. The transaction from the average curve to either the discharge or the charge curve is modeled via a dynamic hysteresis model described in the following paragraph.[5]

4.3.3. Hysteresis model

Following the approach proposed in Refs. [17], the hysteresis is modeled by:

$$\dot{h}(t) = \left|\frac{\eta\gamma i_{\mathrm{batt}}(t)}{Q_{\mathrm{batt}}}\right| \cdot (M(\mathrm{SoC}, \mathrm{sign}(i_{\mathrm{batt}})) - h(t)) \tag{4}$$

where:

- η is the battery efficiency;
- M(SoC,sign(i_{batt})) is the hysteresis steady state gain, defined as half of the difference between the two charge/discharge curves and the v_{oc}. It is negative in charge (i_{batt}<0) and positive in discharge (i_{batt}>0);
- γ is a constant parameter; γ determines the speed of the hysteresis phenomenon, *i.e.* of the switching between the two v_{oc} characteristics. It is estimated from the voltage response to current direction changes, through an optimization procedure which is implemented through the MATLAB PEM identification routine [36]. An average value of 0.067 is estimated for γ.

[3] Q_{batt} may be either the nominal value declared by the manufacturer in the datasheet, or a value identified through a capacity test.

[4] A lengthy procedure: the battery is discharged with a very low current, and at regular intervals (say 10% SoC) the discharge is interrupted and the battery dwells for several hours. The voltage reached at the end of the rest is the v_{oc} at that given SoC. the same procedure may be repeated in charge.

[5] It should be said that the simplest way to involve the hysteresis in the battery model is to switch between charge and discharge characteristics, based on the current direction. The instantaneous switching between the two characteristics is a rough approximation, which yet can be admitted if the changes in current direction are quite rare. If the application requires frequent switching, like Start&Stop application investigated in this work, it is worth to use a proper model of the electrochemical hysteresis dynamics.

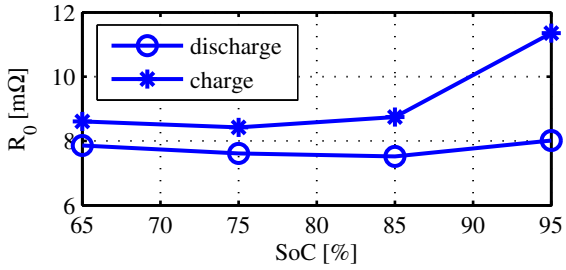

Fig. 8. Estimated values of battery R_0 resistance in charge and discharge as a function of SoC, as computed from Equation (3).

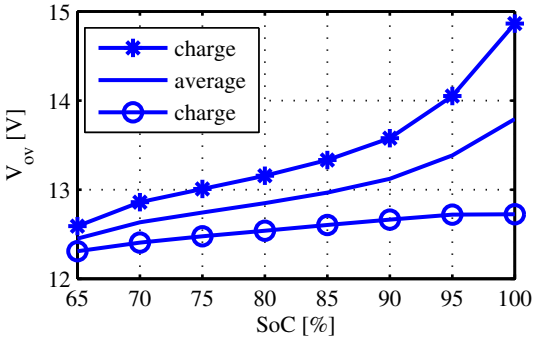

Fig. 9. Battery open circuit voltage estimation: Discharge, charge and average open circuit voltage curves.

4.3.4. R_1 and C_1 identification

The voltage across the *RC* parallel branch (v_1) models the transient response of the output voltage and is given by:

$$R_1 C_1 \, \dot{v}_1(t) = -v_1(t) + R_1 i_{\text{batt}}(t) \tag{5}$$

Similarly to what was done for γ, both R_1 and C_1 are estimated from the voltage response to the current pulses, through MATLAB PEM identification routine [36]. The resulting values are plotted in Fig. 10 and Fig. 11.

In Fig. 12 the voltage measured during the pulse test and the voltage predicted by our model are compared. The root mean square value of the model error is 82.9 mV.

5. DLC

The simplest equivalent electric circuit model for a DLC is a 1st order model consisting of a capacitor and a resistor connected in series (RC), which models the non-ideal ohmic losses of the device. This model can in general well reproduce the electrical behavior of a DLC over a time scale of several seconds. In order to get more accurate results over longer time scales, higher order models should be used. This is achieved by connecting further RC branches in parallel to the original RC branch [20,21]. Each RC branch is responsible to modeling the DLC over a different time scale, from the slowest (seconds) to the fastest (minutes) [9].

A 2nd order, parallel branch model has been selected in this work to represent the dynamic behavior of the DLC. With reference to Fig. 13, the $R_f C_f$ branch captures the fast dynamics of the order of few seconds, whereas the R_d C_d branch is responsible for the delayed dynamics of minutes.

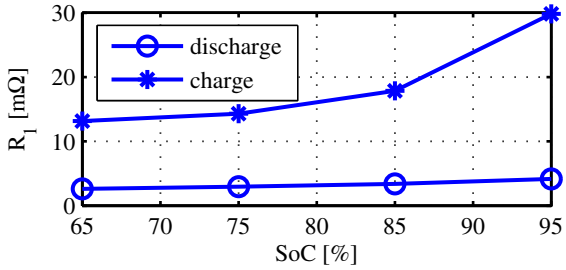

Fig. 10. Estimated values of battery R_1 resistance in charge and discharge as a function of SoC.

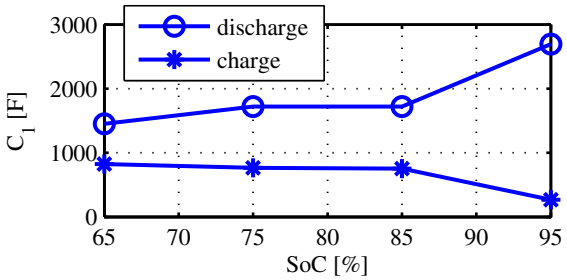

Fig. 11. Estimated values of battery C_1 capacitance in charge and discharge as a function of SoC.

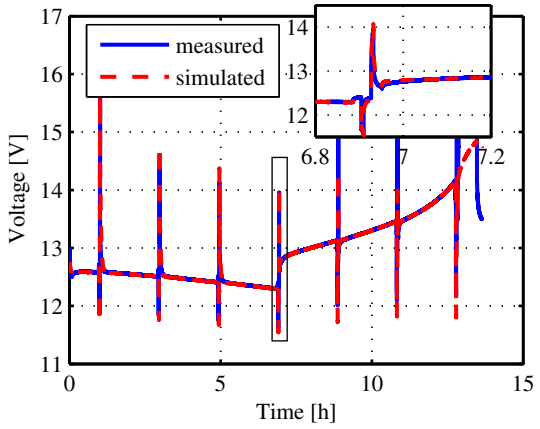

Fig. 12. Battery model validation.

5.1. DLC testing

The identification tests are performed in an environmental chamber at three different temperatures (−18 °C, 25 °C, 50 °C). The testing protocol, shown in Fig. 14, is as follows:

1. the DLC is charged at constant current (100 A) until the voltage reaches the rated voltage (2.7 V);
2. 15 s of dwell;
3. the DLC is discharged at constant current (100 A) until the voltage reaches 50% of the rated voltage (1.35 V);
4. 15 s of dwell;

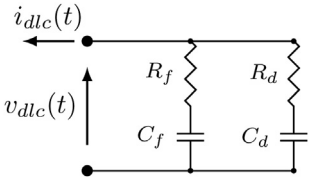

Fig. 13. DLC 2nd equivalent electric circuit model.

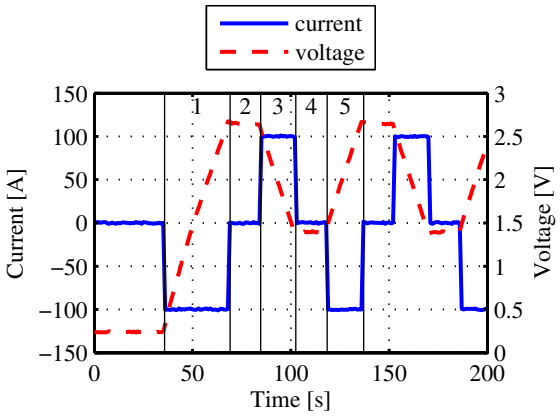

Fig. 14. DLC electric model identification: Current and voltage profile measured at 25 °C.

5. the DLC is charged at constant current (100 A) until the voltage reaches the rated voltage (2.7 V);

Steps 2–5 are performed 50 times for each testing temperature.

5.2. DLC electric model identification

The voltages across the capacitors are described by the following differential equations:

$$\dot{v}_{Cf} = \frac{1}{C_f} i_f \tag{6}$$

$$\dot{v}_{Cd} = \frac{1}{C_d} i_d \tag{7}$$

By Kirchhoff Current Law, the current entering in the device is:

$$i_{\mathrm{dlc}} = i_f + i_d \tag{8}$$

and the voltage across the device is:

$$v_{\mathrm{dlc}} = i_f R_f + v_{Cf} = i_f R_d + v_{Cd} \tag{9}$$

In principle, the four parameters of this model (R_f, R_d, C_f and C_d) depend on SoC, temperature, current magnitude and direction. In reality, though, experimental evidence, results from the literature and also DLC manufacturer data sheet [35] show that the DLC model parameters need to be scheduled with respect to the temperature only, as the other variables do not seem to have any influence on these parameters.[6]

Raw guesses for the model parameters are calculated according to time-domain methods found in Refs. [9]; those guesses are then refined through a global optimization procedure which was implemented using the MATLAB PEM identification routine [36]. The resulting parameters for the model at the three temperatures are shown in Figs. 15 and 16.

[6] It shall also be pointed out that in Ref. [9] was suggested that the value of C_f depends on the voltage across the capacitor itself v_{cf}. In this case the model is able to capture the non-linear rise of voltage that some devices show during a constant current charge; nevertheless, the model becomes non-linear. We neglected this possible dependence, since the DLC is expected to operate in a narrow voltage range, quite close to the maximum allowed voltage (when used in Start&Stop application the DLC voltage is between about 1.9 and 2.4 V, as one can see in Fig. 22).

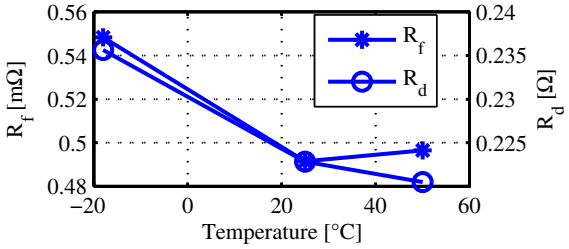

Fig. 15. Estimated values of the DLC R_f and C_dR_d resistances.

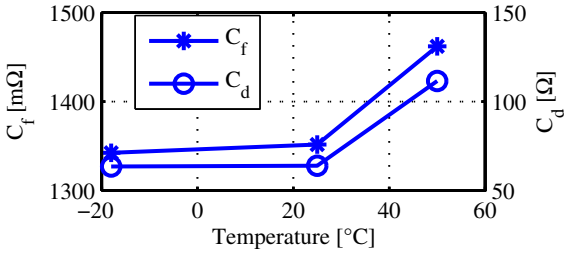

Fig. 16. Estimated values of the DLC C_f and capacitances

In Fig. 17 the measured DLC voltage is compared with the voltage predicted by our model, for the test at 25 °C. The RMS error is 27.7 mV.

5.3. DLC thermal model identification

The purpose of thermal model is to estimate the surface temperature of the device based on the measurements of the air temperature and of the current. Notice that the electrical model and the thermal model are deeply related to one another. The parameters of the electrical model depend on the surface temperature predicted by the thermal model. On the other hand, the equivalent heat of the thermal model depends on the current and voltage predicted by the electrical model.

The temperature of the DLC is assumed to be homogeneous and influenced only by the self-generated heat and by the ambient temperature, assumed to be homogeneous as well. The generated heat Q_{gen}, related to the power losses in the device, is given by:

$$Q_{\mathrm{gen}} = \begin{cases} i_{\mathrm{dlc}}^2 R, & i_{\mathrm{dlc}} > 0 \quad \text{(discharge)} \\ i_{\mathrm{dlc}}^2 R - i_{\mathrm{dlc}} v_{\mathrm{dlc}} (1-\eta), & i_{\mathrm{dlc}} < 0 \quad \text{(charge)} \end{cases} \tag{10}$$

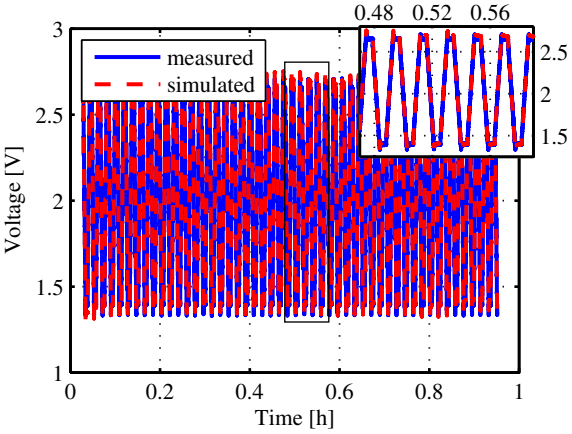

Fig. 17. DLC electric model simulation.

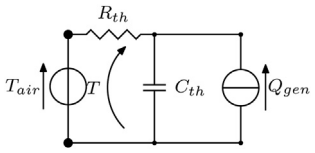

Fig. 18. DLC thermal model equivalent electric circuit.

where R is the equivalent series resistance of the device, which can be fairly approximated with R_f, and η is its charging efficiency.

For the sake of simplicity, a 1st order model (Fig. 18) is assumed for the thermal response of the DLC to self-generated heat Q_{gen} and to ambient temperature T_{air}:

$$C_{\text{th}}\dot{T}_{\text{dlc}} + \frac{1}{R_{\text{th}}}T_{\text{dlc}} = \frac{1}{R_{\text{th}}}T_{\text{air}} + Q_{\text{gen}} \tag{11}$$

where:

- T_{dlc} is the surface temperature [°C];
- R_{th} is the thermal resistance (*i.e.* the reciprocal of thermal conductance) of the DLC for exchanges between the surface and the ambient [W^{-1}°C];
- C_{th} is the thermal capacitance of the DLC, *i.e.* the amount of heat required to change its temperature by a given amount [$°C^{-1}$ J].

Both R_{th} and C_{th} are parameters provided by the manufacturer, reported in Table 2. The simulation of the thermal model is shown in Fig. 19. The root mean square value of the simulation error is 0.247 °C.

6. HESS

Adding the DLC module to the battery allows to increase the power of the overall energy storage system with respect to the stand-alone battery. The number of device's series is selected in order to avoid that the maximum rated voltage across the battery exceeds the maximum rated voltage across the DLC module. If this constraint is violated the DLC experience an over-voltage situation and then can lead to serious damage. In a module with six devices in series, the maximum rated voltage for the DLC module is 16.2 V which is more than the maximum rated voltage of the battery (16 V). As for the number of modules connected in parallel, it is chosen to provide to the overall system enough capacitance to accomplish the energy requirements for the application. In this case, the battery provides enough energy, therefore a single DLC module is adequate.

The model of the HESS is obtained by connecting in parallel the models of the battery and of the six-cells DLC module, as shown in the schematic of Fig. 20. The equations describing the HESS are obtained from the equations of the electrical models of the battery and the DLC; The physical connections between the devices generate the following equations:

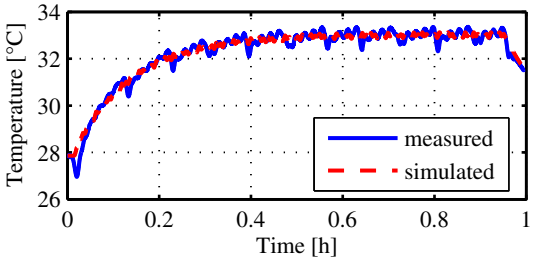

Fig. 19. DLC thermal model simulation.

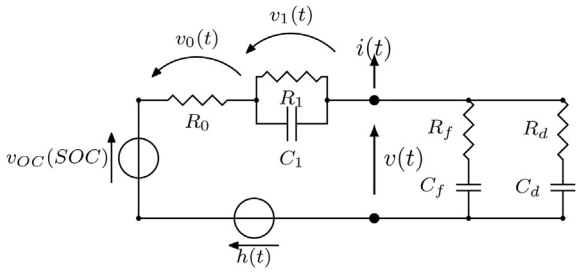

Fig. 20. HESS equivalent circuit model.

$$v = v_{\text{batt}} = v_{\text{dlc}} \tag{12}$$

$$i = i_{\text{batt}} + i_{\text{dlc}} = i_{\text{batt}} + i_f + i_d \tag{13}$$

which lead to the HESS model equations:

$$\begin{cases} \dot{v}_{Cf} = \dfrac{1}{C_f} i_f \\ \dot{v}_{Cd} = \dfrac{1}{C_d} i_d \\ \dot{v}_1 = \dfrac{R_1}{1 + sR_1C_1} i_{\text{batt}} \\ \dot{h} = \dfrac{\eta\gamma}{Q_{\text{batt}}} |i_{\text{batt}}|(M - h) \\ \text{SȯC} = \dfrac{1}{3600 Q_{\text{batt}}} i_{\text{batt}} \end{cases} \tag{14}$$

6.1. HESS model validation

The experimental validation of the HESS system is made by a test illustrated in Fig. 21. The validation current profile has been designed aiming to reproduce the operating conditions that the device would undergo in a vehicle equipped with the Start&Stop technology. This technology requires to start the engine much more frequently than in a conventional vehicle, which can result in accelerated aging of the battery. This may boost the adoption of HESSs as an alternative storage system to conventional batteries.

The Start&Stop current profile protocol, shown in Fig. 21, consists of 30 repetitions of the following cycle:

- discharge @ 45 A for 59 s. This represents the current required to the battery during the normal vehicle operation, when the

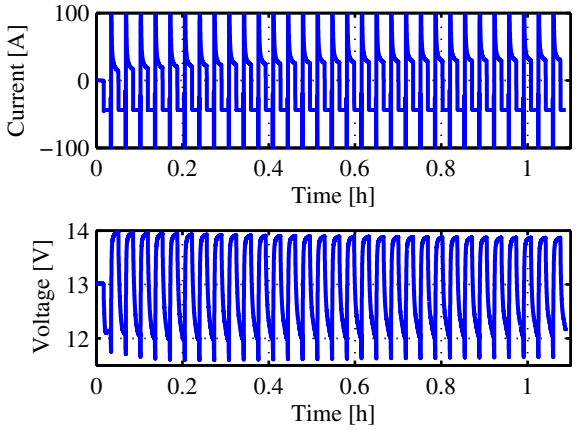

Fig. 21. Start&Stop current and voltage profiles.

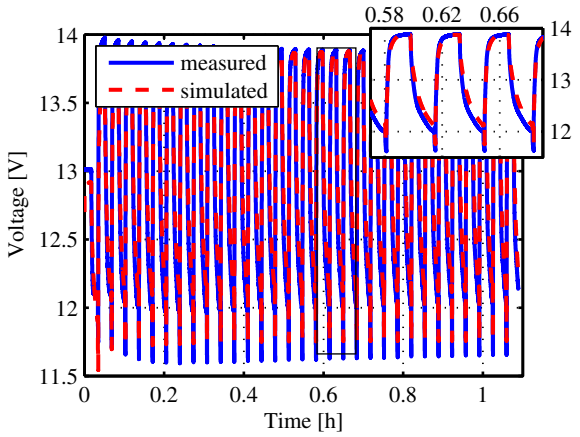

Fig. 22. HESS model validation: v comparison.

alternator cannot provide all the current absorbed by the electrical loads;
- discharge @ 100 A for 3 s. This represents the cranking current peak required to start the warm engine;
- 60 s charge, in order to approximately bring the SoC back to the value it had at the beginning of the cycle, and therefore to operate the Start&Stop cycle at normally the same SoC.

In Fig. 22 a comparison between the measured voltage and the simulated voltage is shown. The RMS error is 152 mV.

In Fig. 23 is shown a comparison between measured and simulated battery current. The RMS of the simulation error is 2.88 A. Fig. 24 shows a comparison between measured and simulated battery current. The RMS error is 2.67 A.

7. HESS combination with the Start&Stop technology

In this section we analyze the feasibility of an HESS in a vehicle equipped with the Start&Stop technology. In order to get an exhaustive comparison between proven and innovative technologies, we performed a simulation study concerning the four following configurations:

- conventional propulsion with a standalone battery;
- conventional propulsion with a HESS;
- Start&Stop technology with a standalone battery;
- Start&Stop technology with a HESS.

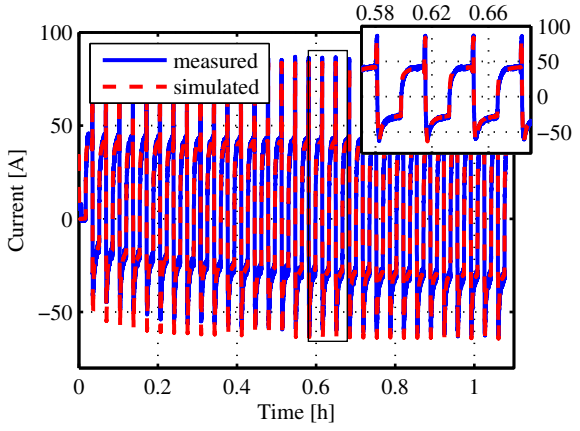

Fig. 23. HESS model simulation: i_{batt} comparison.

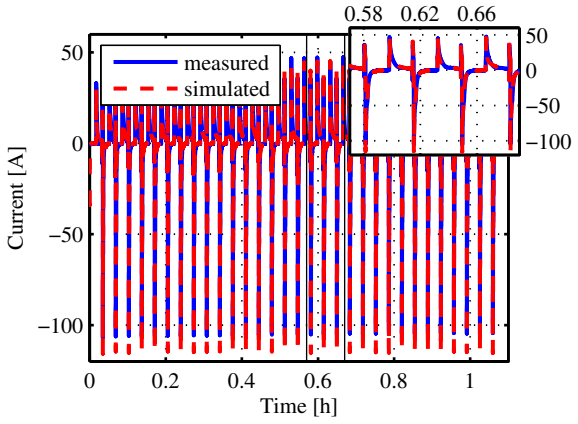

Fig. 24. HESS model simulation: i_{dlc} comparison.

For this study, a detailed simulator of a vehicle powered by an internal combustion engine is used. Due to copyright reasons, details of this simulator cannot be divulged; however it relies on the physical principles underlying the vehicle dynamics, the combustion processes in the engine, the torque transmission, the Electric Power Generation and Storage System and all the supervising controls, including the human driver.

The input to the simulator is the velocity profile that the vehicle has to follow; we conducted our study with the velocity profile of the Federal Testing Procedure driving cycle. Moreover, the current profiles absorbed by the on-board loads can be specified by the user. Although the simulator was originally developed for an SUV, yet our analysis has a general validity, regardless of the vehicle size.

The following figures of merit are introduced for a comparison analysis between the four selected scenarios:

- the ratio between the 1-norm[7] of the current flowing in the battery and the total current flowing in the ESS, $J_1 = \|i_{\text{batt}}(t)\|_1 / \|i_{\text{ess}}(t)\|_1$; J_1 attempts at describing the current splitting between battery and DLC in the HESS with respect to the total current in/out the ESS. From a physical standpoint, it is the ratio between the charge throughputs of the battery and the ESS charge throughput.
- the ratio between the 2-norm[8] of the current flowing in the battery and the total current flowing in the ESS, $J_2 = \|i_{\text{batt}}(t)\|_2 / \|i_{\text{ess}}(t)\|_2$; J_2 attempts at describing the energy splitting between battery and DLC in the HESS with respect to the total energy in/out the ESS. From a physical standpoint, it is the ratio between the energy processed by the battery and the ESS processed energy.
- the fuel consumption, expressed in miles per gallon, in order to verify that it is reduced by the Start&Stop technology.

The fuel consumption is related to the instantaneous power of the engine P_{eng} by:

$$P_{\text{eng}} = T_{\text{eng}}\omega_{\text{eng}}\eta_{\text{eng}} = \dot{m}_{\text{fuel}}\lambda \tag{15}$$

where:

- T_{eng} is the torque supplied by the engine;
- ω_{eng} is the engine speed;
- η_{eng} is the engine efficiency;
- $\dot{m}_{\text{fuel}}$ is the fuel mass flow;
- λ is the fuel lower heating value.

[7] The 1-norm is defined as $\|x(t)\|_1 = \int_0^t |x(\tau)| d\tau$.
[8] The 2-norm is defined as $\|x(t)\|_2 = \int_0^t x^2(\tau) d\tau$.

Table 3
Simulation results.

	Battery			HESS		
	J_1	J_2	*mpg*	J_1	J_2	*mpg*
Conventional	1	1	18.56	0.79	0.51	18.53
Start&Stop	1	1	19.60	0.78	0.54	19.56

The total mass of consumed fuel is given by $m_{\text{fuel}} = \int_0^t \dot{m}_{\text{fuel}}(\tau)\mathrm{d}\tau$. The engine torque T_{eng} compensates all the load torques, including tire friction resistance, aerodynamic resistance, vehicle inertia and the alternator torque:

$$T_{\text{eng}} = \sum T_{\text{res}} + T_{\text{alt}} \tag{16}$$

where $T_{\text{alt}} = Ki_{\text{alt}}$ is the alternator torque, proportional to the alternator current i_{alt}. The current required to either the battery or the HESS results from the difference between the alternator current i_{alt} itself and the load current i_{load}, which is required for the engine starting and for the additional electric loads.

The voltage of the energy storage system (battery or HESS) is regulated to a reference value by means of a closed loop control system.

Table 3 summarizes the results of the simulation study. With a Federal Testing Procedure driving cycle, our simulator predicts a significant relief of the battery when the HESS is used. Both with the conventional and with the Start&Stop technology, the charge that the battery is required to process is reduced by 20%, as indicated by figure J_1. In a similar way, the energy processed is reduced by 50%, as indicated by figure J_2. On the other hand, the Start&Stop technology reduces the fuel consumption by 5%, regardless of the energy storage system used. Actually, the simulations show that changing the energy storage system (battery or HESS) results in a negligible difference in the fuel consumption (Table 3).

The HESS turns out to be a good solution to mitigate the stress on the battery when a Start&Stop is used. If the only concern is to limit the fuel consumption, the Start&Stop technology can be conveniently used with a standalone battery, which however will undergo more stressful operating conditions, and therefore accelerated aging.

8. Conclusions

In this paper, a model of a passive HESS intended for automotive applications and consisting of a PbA battery and DLCs has been proposed. We developed and experimentally identified dynamic circuit-based models of a PbA battery and of the DLC. The two models have then been used to develop the HESS model which has been experimentally validated by means of a current profile, mimicking the likely operating conditions in a vehicle equipped with the Start&Stop technology. Good agreement was found between the measurements of the HESS voltage, of the battery current and of the DLC current and the corresponding signals predicted by the HESS model. The validated model of the HESS and of the standalone battery were used in a vehicle simulator to perform a comparative analysis of the fuel consumption obtained when the vehicle uses the HESS vs. the standalone battery as energy storage system. Moreover, evaluation of battery stress under different scenarios (standalone vs. HESS and Start&Stop vs. conventional powertrain) was performed. The study showed that:

- the Start&Stop technology comes with a significant reduction of the fuel consumption (about 5% with the selected driving cycle), regardless of the energy storage system (battery or HESS) adopted in the vehicle;
- if a standalone battery is used, the Start&Stop technology results in a more aggressive operating condition, with a detrimental effect on the battery life;
- if a HESS is used, the impact of the Start&Stop technology on the battery aging is mitigated with respect to the case of standalone battery, as it is shown by figures of merit J_1 and J_2 which are reduced in the order of 20% and 50% respectively. Besides mitigating the battery aging, the adoption of an HESS may also allow to downsize the battery.

Acknowledgments

The authors would like to thank MIDAC Batteries S.p.A. in the persons of Nullo Madella, Stefano Bovo and Andrea Saletti for the financial support under which the work presented here was conducted and for kindly donating the batteries used in this project.

References

[1] J.M. Miller, Propulsion Systems for Hybrid Vehicles, IET, 2004.
[2] DOE – Fossil Energy: DOE's Fuel Cell R&D Program (2012).
[3] D. Pavlov, Lead-acid Batteries: Science and Technology, Elsevier Science, 2011.
[4] G. Rizzoni, H. Peng, vol. 1, DSCC Magazine, to be issued in 2013.
[5] P. Mauracher, E. Karden, Journal of Power Sources 67 (1997) 69–84.
[6] M. Ceraolo, IEEE Transactions on Power Systems 15 (2000) 1184–1190.
[7] Z. Salameh, M. Casacca, W. Lynch, IEEE Transactions on Energy Conversion 7 (1992) 93–98.
[8] L. Shi, M.L. Crow, in: Power and Energy Society General Meeting – Conversion and Delivery of Electrical Energy in the 21st Century, IEEE, 2008, pp. 1–6.
[9] L. Zubieta, R. Bonert, IEEE Transactions on Industry Applications 36 (2000) 199–205.
[10] S. Buller, E. Karden, D. Kok, R. De Doncker, in: Industry Applications Conference – 36th IAS Annual Meeting, vol. 4, IEEE, 2001, pp. 2500–2504.
[11] S. Buller, M. Thele, R. De Doncker, E. Karden, IEEE Transactions on Industry Applications 41 (2005) 742–747.
[12] Z. Li, J. Chen, Microelectronic Engineering 85 (2008) 1549–1554.
[13] F. Belhachemi, S. Rael, B. Davat, in: Industry Applications Conference, vol. 5, IEEE, 2000, pp. 3069–3076.
[14] J. Marie-Francoise, H. Gualous, A. Berthon, in: IEE Proceedings on Electric Power Applications, vol. 153, IET, 2006, pp. 255–262.
[15] V. Srinivasan, J. Weidner, Journal of the Electrochemical Society 146 (1999) 1650–1658.
[16] G. Sikha, R. White, B. Popov, Journal of The Electrochemical Society 152 (2005) 1682–1693.
[17] G. Plett, Journal of Power Sources 134 (2004) 262–276.
[18] J. Van Mierlo, P. Van den Bossche, G. Maggetto, Journal of Power Sources 128 (2004) 76–89.
[19] J. Marie-Francoise, H. Gualous, R. Outbib, A. Berthon, Journal of Power Sources 143 (2005) 275–283.
[20] K. Do, A Dynamic Electro-thermal Model of Double Layer Supercapacitors for HEV Powertrain Applications. Ph.D. thesis, Ohio State University, 2004.
[21] K.M. Do, A Dynamic Electro-thermal Model of Double Layer "Supercapacitors" for HEV Powertrain Applications, MSc Thesis, The Ohio State University, 2004.
[22] X. Hu, S. Li, H. Peng, Journal of Power Sources 198 (2012) 359–367.
[23] P. Bentley, D. Stone, in: European Conference on Power Electronics and Applications, IEEE, 2005, pp. 10–20.
[24] H. Catherino, J. Burgel, P. Shi, A. Rusek, X. Zou, Journal of Power Sources 162 (2006) 965–970.
[25] A. Stienecker, T. Stuart, C. Ashtiani, Journal of Power Sources 156 (2006) 755–762.
[26] A. Baisden, A. Emadi, IEEE Transactions on Vehicular Technology 53 (2004) 199–205.
[27] S. Lukic, S. Wirasingha, F. Rodriguez, J. Cao, A. Emadi, in: Vehicle Power and Propulsion Conference, IEEE, 2006, pp. 1–6.
[28] E. Schaltz, A. Khaligh, P. Rasmussen, IEEE Transactions on Vehicular Technology 58 (2009) 3882–3891.
[29] R. Dougal, S. Liu, R. White, IEEE Transactions on Components and Packaging Technologies 25 (2002) 120–131.
[30] L. Gao, R. Dougal, S. Liu, in: Applied Power Electronics Conference and Exposition, vol. 1, IEEE, 2003, pp. 497–503.
[31] H. Gualous, D. Bouquain, A. Berthon, J. Kauffmann, Journal of Power Sources 123 (2003) 86–93.
[32] L. Gao, R. Dougal, S. Liu, IEEE Transactions on Power Electronics 20 (2005) 236–243.
[33] D. Cericola, P. Ruch, R. Kotz, P. Novak, A. Wokaun, Journal of Power Sources 195 (2010) 2731–2736.
[34] Midac Batteries Official Website (2012).
[35] Maxwell Technologies Official Website (2012).
[36] Prediction Error Estimate of Linear or Nonlinear Model – MATLAB (2012).